water

MDPI

Article

Comparison of IMERG Level-3 and TMPA 3B42V7 in Estimating Typhoon-Related Heavy Rain

Ren Wang [1,2], Jianyao Chen [1,2,*] and Xianwei Wang [2,*]

[1] Department of Water Resources and Environment, School of Geography and Planning, Sun Yat-sen University, Guangzhou 510275, China; rwang91@foxmail.com

[2] Guangdong Key Laboratory for Urbanization and Geo-simulation, Sun Yat-sen University, Guangzhou 510275, China

* Correspondence: chenjyao@mail.sysu.edu.cn (J.C.); wangxw8@mail.sysu.edu.cn (X.W.); Tel.: +86-20-8411-5930 (J.C.)

Academic Editor: Ataur Rahman
Received: 17 January 2017; Accepted: 10 April 2017; Published: 22 April 2017

Abstract: Typhoon-related heavy rain has unique structures in both time and space, and use of satellite-retrieved products to delineate the structure of heavy rain is especially meaningful for early warning systems and disaster management. This study compares two newly-released satellite products from the Integrated Multi-satellitE Retrievals for Global Precipitation Measurement (IMERG final run) and the Tropical Rainfall Measuring Mission (TRMM) Multi-satellite Precipitation Analysis (TMPA 3B42V7) with daily rainfall observed by ground rain gauges. The comparison is implemented for eight typhoons over the coastal region of China for a two-year period from 2014 to 2015. The results show that all correlation coefficients (*CCs*) of both IMERG and TMPA for the investigated typhoon events are significant at the 0.01 level, but they tend to underestimate the heavy rainfall, especially around the storm center. The IMERG final run exhibits an overall better performance than TMPA 3B42V7. It is also shown that both products have a better applicability (i.e., a smaller absolute relative bias) when rain intensities are within 20–40 and 80–100 mm/day than those of 40–80 mm/day and larger than 100 mm/day. In space, they generally have the best applicability within the range of 50–100 km away from typhoon tracks, and have the worst applicability beyond the 300-km range. The results are beneficial to understand the errors of satellite data in operational applications, such as storm monitoring and hydrological modeling.

Keywords: IMERG final run; TMPA 3B42V7; typhoon; heavy rain; coastal region of China

1. Introduction

Heavy rain events have profound impacts on human society, hydrological processes, and natural ecosystems [1,2]. They can adjust river regimes, flood peak, and waterlogging patterns rapidly, and even cause significant losses in human life and social economy [3–5]. A typhoon is a type of cyclone formed in the tropical ocean and often brings heavy rainfall to coastal territory. Typhoon-related heavy rain has unique patterns in both time and space, e.g., it can last from one day to several days, and is dominated by typhoon track, translation speed, atmospheric environment, etc. Therefore, reliable measurements of the heavy rainfall provide essential information to monitor and forecast its changing patterns, which are crucial for early warning systems and disaster management strategies [6–9]. Moreover, detailed regularity of heavy rainfall across different spatiotemporal scales leads to insights about the variability of runoff, which can further contribute to reduce inundation of urban regions [10]. However, rainfall is highly variable in both space and time during a typhoon event, creating significant challenges in its accurate monitoring.

Radar and satellite precipitation measurements provide more homogeneous datasets than ground gauge observations [11,12]. Radar precipitation estimates are constrained by the monitoring scope of radar, while satellite precipitation products have advantages in global coverage and fine resolution [13,14]. There are currently various open access satellite-based precipitation products that could bring valuable scientific and societal benefits. Meanwhile, those products often contain large uncertainties and inevitable errors in different aspects, such as the variability of the precipitation fields and systematic errors [15–17]. These various errors and differential resolutions influence the accuracy of hydrological modeling [18,19]. Evaluation of these products is, therefore, necessary for further understanding of their error characteristics, and is vital to algorithm improvement and subsequent applications.

The Global Precipitation Measurement (GPM) mission, which was launched on 27 February 2014, provides the next generation satellite-based global observations of rainfall and snow. GPM is built upon the success of the Tropical Rainfall Measuring Mission (TRMM). Currently, the accessible Integrated Multi-satellitE Retrievals for GPM (IMERG) Level-3 products have finer resolutions ($0.1^\circ \times 0.1^\circ$, 30 min) than the TRMM precipitation series ($0.25^\circ \times 0.25^\circ$, 3 h), and are valuable for applications over the band of 60° N to 60° S [20]. Meanwhile, the TRMM Multi-satellitE Precipitation Analysis (TMPA) products have provided abundant precipitation information since 1997 [12]. The recently-updated version, 3B42 version 7 (3B42V7), comprises near-real-time and research-grade products with a resolution of $0.25^\circ \times 0.25^\circ$ in space and 3 h in time [21,22].

Scientists, worldwide, have been investigating the error characteristics of the satellite precipitation series at different spatial and temporal scales. Some studies [6,17,23] demonstrated that TMPA 3B42V7 performs better than TMPA 3B42V6, while both products have larger errors in mountainous regions [6,8]. Some other studies [24–30] made comparisons between IMERG and TMPA products, and reported that IMERG generally exhibits an overall better performance than TMPA, especially for estimating heavy and light precipitation. However, IMERG still has room to improve, such as in arid and high-latitude zones [26,29], and mountainous areas [28,31]. These studies provide a large amount of information to understand the applicability of IMERG and TMPA, but tend to focus on annual, seasonal, and monthly scales, not sufficient for short-term heavy rainfall events, especially when associated with the tropical cyclone rainfall system [4,32]. Evaluation of the products for heavy rainfall is a high standard to verify their performance, and is important in practical applications, such as flood forecasting and urban stormwater collection.

The coastal region of China has experienced frequent typhoons and encountered severe socio-economic losses. In general, typhoons strike the coastal region frequently during the period of July to September every year and generate a large number of rainstorm events. There were more than $5.3 billion economic losses per year since 2001, and approximately 34 typhoons landed in this region, which caused 422 losses to life during 2011–2015 [33]. It is of great significance to focus on typhoon heavy rains over the coastal region of China.

Therefore, our motivations are: (1) to evaluate the performance of two recently-released products, i.e., the IMERG final run and TMPA 3B42V7, in estimating typhoon-related heavy rain over the coastal region of China; and (2) to analyze their applicability with respect to different rainfall intensities and ranges away from the typhoon track. This paper is organized as follows: Section 2 describes the study area and datasets; Section 3 describes the statistical methods used in this study; Section 4 presents and analyzes the results; Section 5 discusses the causes of the error characteristics and the comparative results; and Section 6 provides a summary and some concluding remarks.

2. Study Area and Datasets

2.1. Study Area

The coastal region of China (18°–38.5° N; 104°5′–123° E), which is located at the leading edge of Eurasia and Pacific Ocean, comprises seven provinces and one city, i.e., Shandong, Jiangsu, Zhejiang,

Fujian, Guangdong, Hainan, and Guangxi provinces and Shanghai city (Figure 1). The region is a typical monsoon climate zone, with annual average precipitation ranging from 550 to 2600 mm, and a decreasing pattern from the south to the north. The temporal distribution of precipitation is also uneven, with more than 70% of the annual rainfall concentrating in summer and autumn, when rainfall is primarily controlled by summer wet monsoons and typhoons. Owing to its rapid urbanization and topographic feature, i.e., the eastern areas are mainly plains and rivers downstream where most of the large cities are located, therefore, the risk of flooding is very high over the developed areas. In addition, the coastal region of China has a well-developed economy and dense distribution of cities and people. According to the 2015 China Statistical Yearbook, the region possessed a total gross domestic product (GDP) of $4.48 trillion, accounting for 48% of the national GDP, and had a total resident population of 459 million, accounting for 34% of the country's total population.

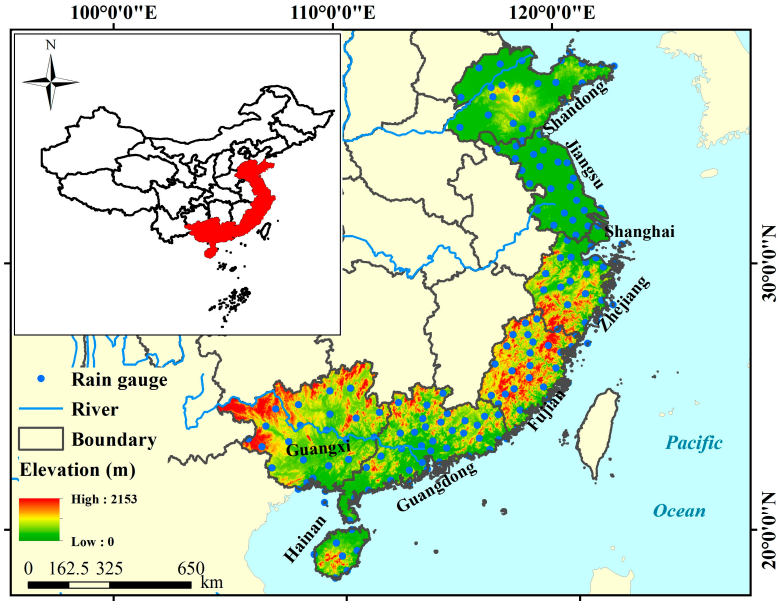

Figure 1. Study area and the spatial distribution of rain gauges.

2.2. Typhoon Events

Eight typhoon events, which landed in the coastal region of China during the two-year period of 2014–2015, are investigated in this study. The study period of 2014 to 2015 is constrained by the availability of the IMERG final run data. Additionally, the investigated typhoons are different in magnitude, typhoon track, duration and the affected geographical areas. The basic information of typhoon events and their storm tracks are obtained from China Typhoon Online [34] and National Meteorological Center [35]. For the convenience of making comparisons, the typhoon events are further divided into two groups according to the geographical areas where they made landfall and their moving directions. Rammasun, Mujigae, Kalmaegi, and Linfa, which made landfall in the southern areas (Guangdong or Hainan province) and moved to the south, are divided into Group I. Chon-hom, Matmo, Soudelor, and Dujuan, which made landfall in the eastern areas (Fujian or Zhejiang province) and moved to the north, are divided into group II. Matmo and Soudelor are two stronger typhoons among them and have almost impacted the entire coastal region. The basic information of the eight investigated typhoons is listed in Table 1.

Table 1. Basic information of the investigated typhoon events over the coastal region of China.

Group	Typhoon Event	Period	Mainly Affected Province (City)	Number of Investigated Station	Maximum Daily Rainfall
Group I	Rammasun	18–19 July 2014	Guangdong, Guangxi, Hainan	55	303.6 mm
	Mujigae	4–5 October 2015	Hainan, Guangdong, Guangxi	58	192.9 mm
	Kalmaegi	16–17 September 2014	Hainan, Guangdong, Guangxi	67	296.5 mm
	Linfa	9–10 July 2015	Guangdong, Fujian	39	158.8 mm
Group II	Chon-hom	11–12 July 2015	Zhejiang, Jiangsu, Fujian, Shanghai	37	267.7 mm
	Matmo	23–25 July 2014	Fujian, Guangdong, Jiangsu, Shandong	98	238.3 mm
	Soudelor	8–10 August 2015	Fujian, Zhejiang, Jiangsu, Guangdong	104	232.1 mm
	Dujuan	28–30 September 2015	Fujian, Zhejiang, Jiangsu	80	170.9 mm

2.3. Gauge Observations

Daily rain gauge observations are collected from the National Meteorological Information Center of the China Meteorological Administration (CMA). There are 165 observation stations in total over the study area (Figure 1) with the gauge density of 1.734 stations per 10^4 km^2. Regarding the data quality control, the dataset has passed homogeneity assessments through the Standard Normal Homogeneity Test method [36]. Non-uniform stations, such as "Shaoguang" "Qingyuan", and "Shangchuandao", have been corrected using the ratio method by CMA. Few missing records, which were amended by the CMA, have been replaced by the mean value of adjacent dates. This study mainly analyzes these stations which had total rainfall larger than 10 mm during a typhoon event and have substantial spatial relation with the typhoon track. Thus, the 10 mm rainfall depth threshold [37], which refers to accumulated rainfall from gauge observations, is applied to screen out the light rainfall since the focus of this study is to investigate the performance of both latest satellite precipitation products for heavy rainfall. In addition, some stations with total rainfall less than 10 mm are still retained if they are within a 150-km range of the typhoon track. One and two stations with rainfall <10 mm have been retained for the Rammasun and Linfa events, respectively.

2.4. TMPA 3B42V7

The latest post real-time 3B42V7 precipitation product of TMPA is used in this study. It integrates various satellite microwave radar data, including that from TRMM Microwave Image (TMI), Special Sensor Microwave Image (SSMI), Special Sensor Microwave Image/Sounder (SSMIS), Advanced Microwave Scanning Radiometer-EOS (AM-SR-E), Advanced Microwave Sounding Unit-B (AMSU-B), and Microwave Humidity Sounder (MHS) [20]. In addition, the 3B42V7 version combines the ground rain gauge products of the Global Precipitation Climatology Center (GPCC) [21]. The improved 3B42V7 data ($0.25^\circ \times 0.25^\circ$, 3 h) are collected from the Precipitation Measurement Missions website [38]. This study utilized all of the TMPA 3B42V7 data, in HDF format, during the period of the typhoons. The unit of the precipitation field is mm per hour, which refers to the precipitation rate. The three-hour 3B42V7 precipitation is further accumulated into daily and event-total rainfall during the period of each typhoon event, based on ENVI version 5.1 which is developed by Exelis Visual Information Solutions company in the United States, and MATLAB R2015a which is developed by MathWorks company in Natick, Massachusetts, USA. The precipitation in a grid that corresponds to the ground gauges can be extracted by ArcMap 10.1 which is provided by Environmental Systems Research Institute in RedLands, California, USA.

2.5. IMERG Final Run

The IMERG final run-calibrated precipitation data are analyzed in this study. The geophysical parameters of IMERG Level-3 have been spatially or temporally re-sampled from Level-1 or Level-2 data, and the Level-3 products include early run, late run, and final run versions. Currently, IMERG employs the 2014 version of the Goddard Profiling Algorithm (GPROF2014) to compute precipitation estimates from all passive microwave (PMW) sensors onboard GPM satellites, and is an improvement

compared to TMPA's retrieval algorithm (GPROF2010) [21,39]. The IMERG final run data [38], with a latency of four months, are available from March 2014 to present, so that the investigated typhoon of this study is constrained in the period of March 2014 to September 2015. All of the IMERG final run datasets in HDF5 format, are collected for the periods of typhoon events. The unit of the precipitation field is mm per half hour. Similar to TMPA 3B42V7, the half-hour IMERG precipitation is also accumulated into daily and event-total rainfall.

3. Methods

A series of common statistical metrics, which include relative bias (*RB*), mean error (*ME*), mean absolute error (*MAE*), root-mean-squared error (*RMSE*), and Pearson linear correlation coefficient (*CC*), are used to perform the comparative evaluation. *RB* is used to evaluate the errors in a gauge-grid pair while *ME*, *MAE*, and *RMSE* are for regional-scale evaluations [40].

RB is the ratio of underestimating or overestimating, in percentage, and it is applicable to reflect errors between the satellite estimates and the corresponding gauge observations. *RB* is calculated for a typhoon event at individual sites by Equation (1):

$$RB_i = \frac{S_i - G_i}{G_i} \times 100 \tag{1}$$

where i is a rain gauge number; S_i represents the satellite precipitation estimates; and G_i represents the gauge observations.

The other metrics (*ME*, *MAE*, and *RMSE*) are used to measure the magnitude of errors for a whole region or sub-region in this study. *MAE* is a statistical metric with absolute value, while *ME* is a metric having positive and negative value, so it can be used to reflect the direction of accumulated errors, i.e., overestimation or underestimation at all stations. Furthermore, *RMSE* is the squared root of errors emphasizing extremes [8]. These statistical metrics can be calculated by Equations (2)–(4):

$$ME = \frac{1}{n}\sum_{i=1}^{n}(S_i - G_i) \tag{2}$$

$$MAE = \frac{1}{n}\sum_{i=1}^{n}|S_i - G_i| \tag{3}$$

$$RMSE = \sqrt{\frac{\sum_{i=1}^{n}(S_i - G_i)^2}{n}} \tag{4}$$

where n represents the number of samples.

In addition, Pearson linear correlation analysis is used to examine the linear agreement of satellite precipitation estimates and rain gauge observations. The *CC* can be obtained by Equation (5) [32].

$$CC = \frac{\sum(x_i - \overline{x})(y_i - \overline{y})}{\sqrt{\sum(x_i - \overline{x})^2 \sum(y_i - \overline{y})^2}} \tag{5}$$

where *CC* is the correlation coefficient, ranging from -1 to 1; $\overline{x} = \frac{1}{n}\sum_{i=1}^{n} x_i$ and $\overline{y} = \frac{1}{n}\sum_{i=1}^{n} y_i$ n represents the number of gauge-grid samples; and x_i and y_i represent the grid-scale satellite measurements and rain gauge observations, respectively.

4. Results

4.1. Characteristics of the Metrics

The statistical metrics (*ME*, *MAE*, RSME, and *CC*), which can reflect the error characteristics of satellite rainfall data over the region during typhoon events, were computed for each gauge-grid pair. The results are presented in Figure 2. With the exception of the products for Mujigae and Rammasun and the IMERG final run for Soudelor, all *MEs* have a negative value, highlighting that both IMERG and TMPA tend to underestimate typhoon heavy rainfall at the regional scale. Moreover, except for the typhoon Dujuan, the absolute *ME* of IMERG is smaller than that of TMPA. Since some samples have large values of positive *RB* (more than 100%), the positive *ME* for Mujigae and Rammasun is highly possible. Meanwhile, there are six typhoon events where the *MAE* of IMERG is slightly larger than that of TMPA. This is also likely to be influenced by some large values of positive *RB* in IMERG. The RSME presents a similar pattern with *MAE*, i.e., RSMEs of IMERG are larger than that of TMPA during the periods of Rammasun, Mujigae, Linfa, Soudelor, and Dujuan. Regarding the correlations between the satellite products and gauge observations, all *CCs* for the investigated typhoon events are significant at the 0.01 confidence level, and there are five typhoon events, i.e., Mujigae, Kalmaegi, Linfa, Soudelor, and Dujuan, that the *CC* of TMPA 3B42V7 is higher than that of the IMERG final run. These larger *CCs* are partially attributed to the smoothing effect of the larger grid size of TMPA (25 km) than IMERG (10 km).

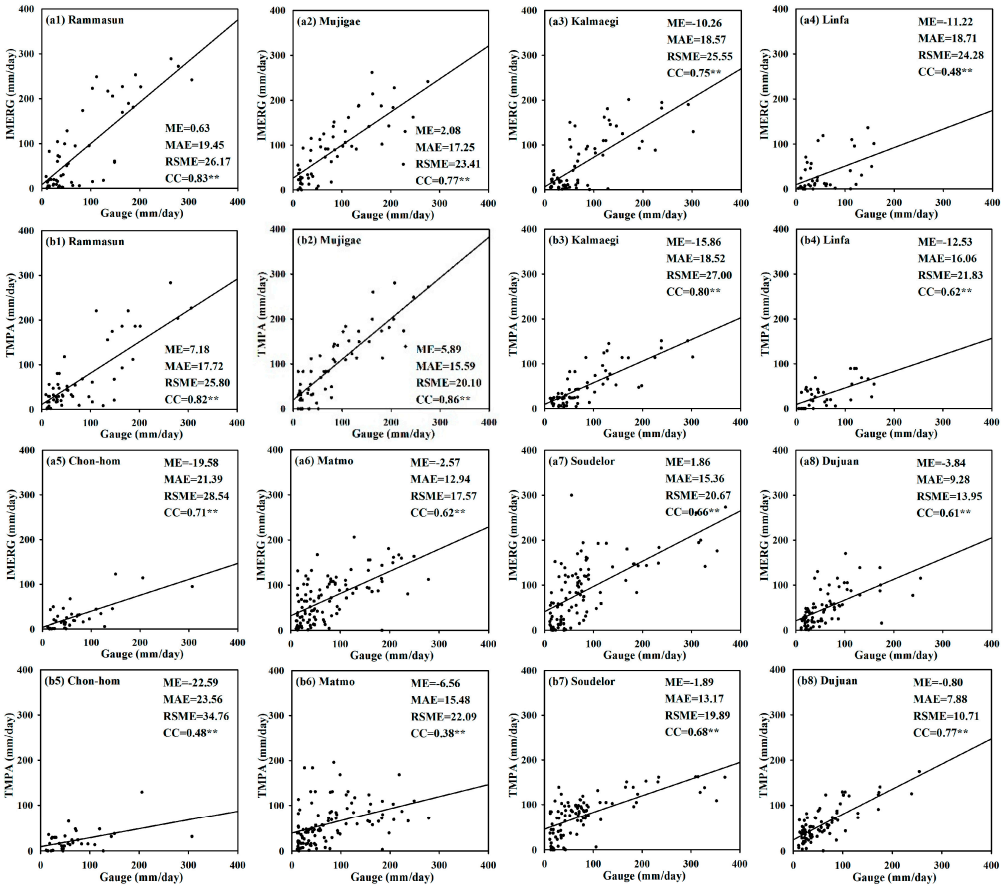

Figure 2. Statistical metrics (*ME*, *MAE*, RSME, and *CC*) of (**a1**–**a8**) the IMERG final run and (**b1**–**b8**) TMPA 3B42V7 against gauge observations for each typhoon event over the coastal region of China. The units of *ME*, *MAE*, and RSME is mm/day, and the range of *CC* is −1 to 1. ** The correlation is significant at the 0.01 level.

Overall, both satellite products underestimate the heavy rainfall at the regional scale. The IMERG final run can provide a slightly better performance than TMPA 3B42V7 in estimating typhoon heavy rainfall. Taking one of the largest typhoon events, Matmo, for example, the Kriging interpolation method [41] was used to map the spatial patterns of total rainfall from gauge observations, as shown in Figure 3. It is also shown that the IMERG final run and TMPA 3B42V7 have captured similar spatial patterns of total rainfall, but they all tend to underestimate the extreme values of total rainfall in the storm center.

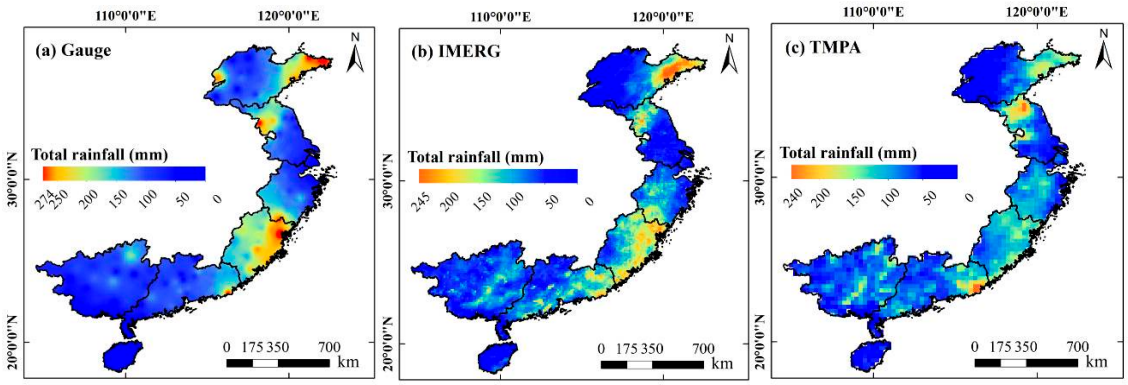

Figure 3. Spatial distribution of total rainfall plotted for (**a**) gauge observations, (**b**) the IMERG final run, and (**c**) TMPA 3B42V7 for typhoon Matmo during the period of 23–25 July 2014.

The characteristics of gauge-grid *RB* of over- and underestimated amounts are illustrated in Figures 4 and 5 for the typhoon events of Group I and Group II, respectively. Table 2 summarizes the percentages of overestimate and underestimate that are illustrated in Figures 4 and 5.

Table 2. The percentage (%) of gauge-grid pairs of over- and underestimation of IMERG and TMPA against gauge observations illustrated in Figure 2.

Typhoon Events		IMERG		TMPA	
		Overestimate	Underestimate	Overestimate	Underestimate
Group I	Rammasun	47.27	52.73	38.18	61.82
	Mujigae	58.62	41.38	67.24	32.76
	Kalmaegi	26.87	73.13	23.88	76.12
	Linfa	25.51	74.49	17.95	82.05
Group II	Chon-hom	8.11	91.89	8.11	91.89
	Matmo	39.80	60.20	35.71	64.29
	Soudelor	55.77	44.23	50.96	49.04
	Dujuan	38.75	61.25	46.25	53.75

The typhoons of group I made landfall in Southern China, such as in Guangdong, Guangxi, or Hainan province. Both IMERG and TMPA underestimated the total rainfall in the storm centers and along the typhoon tracks (Figure 4). For instance, the percentages of IMERG and TMPA's underestimated samples are 74.49% and 82.05% for typhoon Linfa, and 73.13% and 76.12% for typhoon Kalmaegi, respectively (Table 2). However, only one exception exists, for typhoon Mujigae, when both products overestimated the total rainfall in most regions and their percent of overestimated samples are 58.62% (IMERG) and 67.24% (TMPA).

The typhoons of group II made landfall in Eastern China (Fujian and Zhejiang provinces) and moved toward northern areas. Similar to Group I, both the IMERG final run and TMPA 3B42V7 show underestimation for the total rainfall in the storm centers (Figure 5). Both products underestimated the total rainfall of most samples for typhoon Chon-hom, and their underestimated percentages

are all 91.89% (Table 2), with different magnitudes of underestimation (Figure 5). This relates to the rain intensity of Chon-hom, as it was a powerful typhoon with a maximum daily rainfall of 267.7 mm (Table 1). Moreover, its track through the coastal areas should also contribute to the largest underestimation. In contrast, for typhoon Soudelor, IMERG and TMPA both displayed larger values than the gauge observations, especially in the east of the typhoon track. Their overestimated samples were 55.77% (IMERG) and 50.96% (TMPA).

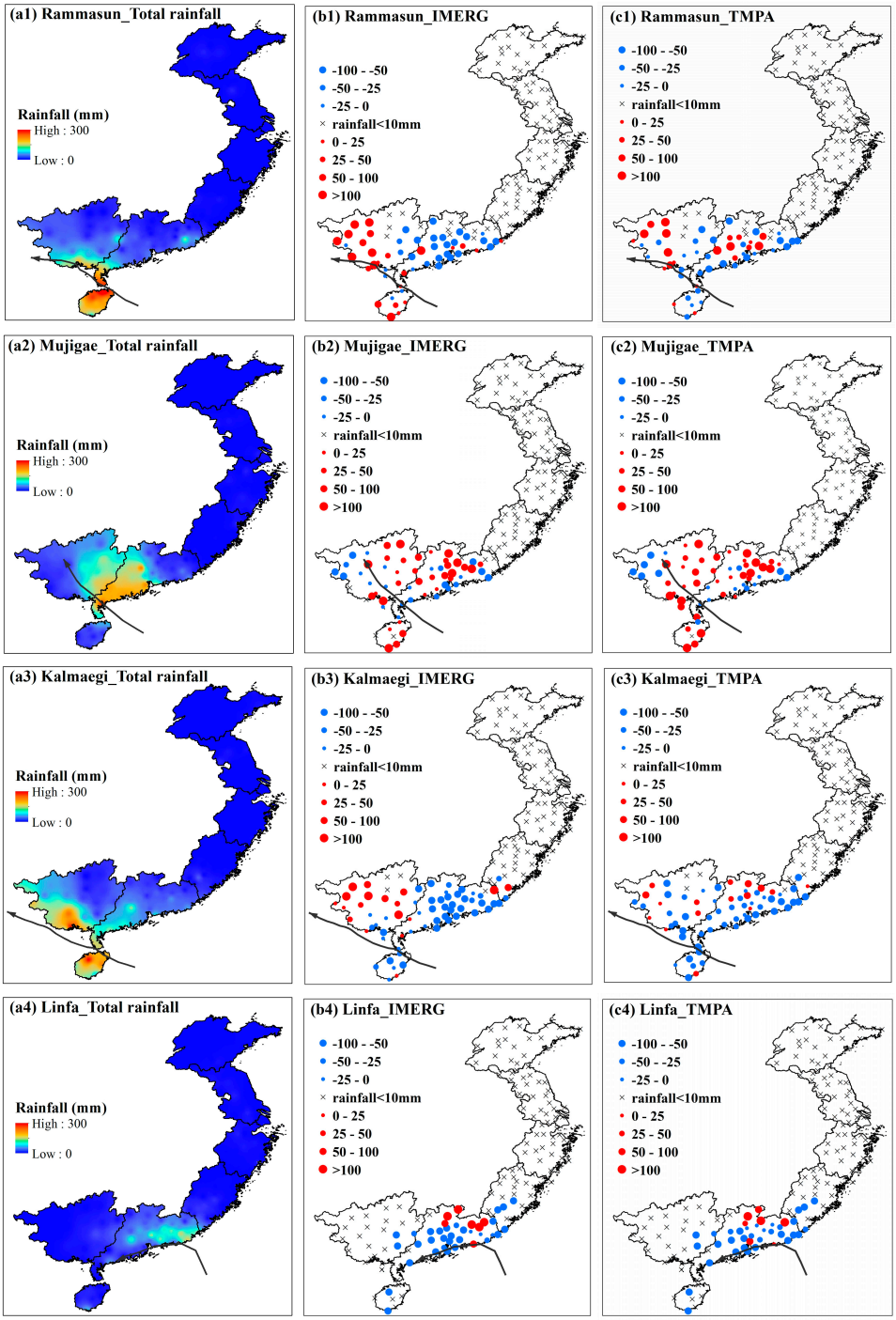

Figure 4. Spatial distribution of total rainfall (**a1**–**a4**), *RB* (%) in (**b1**–**b4**) IMERG and (**c1**–**c4**) TMPA for the typhoon events of Group I (Rammasun, Kalmaegi, Linfa, and Mujigae). Dots are scaled according to the magnitude of the overestimation or underestimation. The arrowed lines represent typhoon tracks.

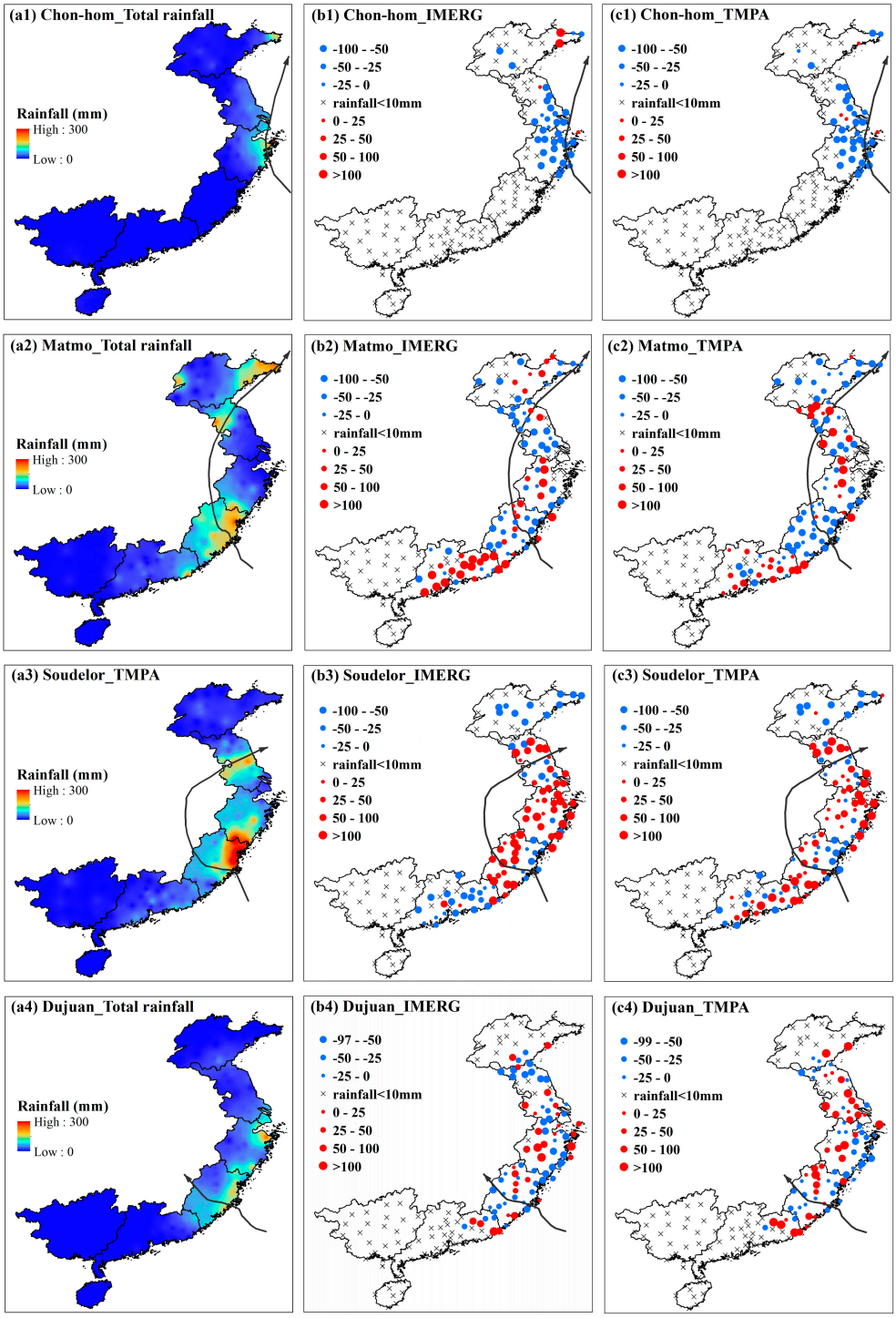

Figure 5. Spatial distribution of total rainfall (**a1**–**a4**), *RB* (%) in (**b1**–**b4**) IMERG and (**c1**–**c4**) TMPA for the typhoons of Group II (Chon-hom, Matmo, Soudelor, and Dujuan). Dots are scaled according to the magnitude of the overestimation or underestimation. The arrowed lines represent typhoon tracks.

4.2. Applicability Associated with Rain Intensity and Typhoon Track

The above analysis indicates that the performance of IMERG and TMPA are associated with the storm center or rain intensity. Therefore, the applicability of the products associated with rain intensity and typhoon track are further investigated. Figure 6 shows that both IMERG and TMPA have many large overestimate samples (*RB* > 100%) when rain intensity is less than 20 mm/day,

and the percentages of IMERG and TMPA's overestimated samples are 44.31% and 54.90%, with mean an *RB* of 31.51% and 45.23% (Table 3). When the rain intensity is larger than 20 mm/day, both IMERG and TMPA capture smaller rainfall than gauge observations, and the magnitude of the underestimation is generally increased with the increased rain intensity. When rain intensities are 20–40 and 80–100 mm/day, the absolute *RB* ($|RB|$) are smaller than those of 40–80 and larger than 100 mm/day. Meanwhile, the $|RB|$ of IMERG are much smaller than those of TMPA in all rain intensity ranges, which again suggest the better performance of IMERG than TMPA.

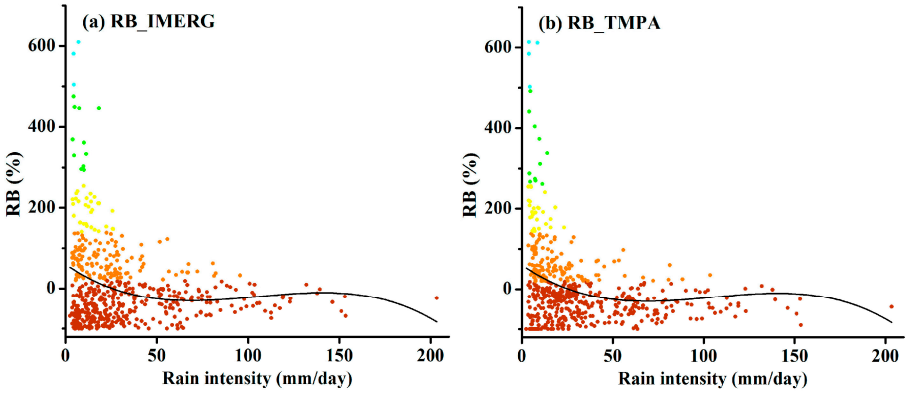

Figure 6. Scatter diagram and fitted curve of the rain intensity and *RB* in (**a**) IMERG final run and (**b**) TMPA 3B42V7 for the eight investigated typhoon events. The colors of the dots represent different magnitudes of *RB*.

Table 3. The percentage (%) of overestimate (over-per) and underestimate (under-per) and mean *RB* (%) in IMERG and TMPA at different rain intensity (mm/day) for the eight typhoon events.

Rain Intensity	IMERG			TMPA		
	Over-Per	Under-Per	*RB*	Over-Per	Under-Per	*RB*
0–20	44.31	55.69	31.51	54.90	45.10	45.23
20–40	39.86	60.14	−9.23	33.11	66.89	−19.58
40–60	33.33	66.66	−12.14	21.57	78.43	−23.77
60–80	18.18	81.82	−27.92	18.18	81.82	−41.13
80–100	50.00	50.00	−7.87	25.00	75.00	−22.50
>100	12.50	87.50	−30.17	12.50	87.50	−34.81

Furthermore, the distance of stations away from the typhoon central track also has an influence on the rain intensity, as well as the performance of satellite rainfall products. As shown in Figure 7, the rain intensity mainly decreases with the increase of the distance from typhoon tracks, which are consistent with storm centers that are around the typhoon tracks (Figures 4 and 5). Meanwhile, the averaged *RB* of both IMERG and TMPA are mainly larger for those stations with a range >300 km than those within smaller ranges. Table 4 shows that IMERG has the smallest absolute mean *RB* in the range of 50–100 km, and has the largest *RB* in a range within 300 km. TMPA also has the smallest absolute mean *RB* in the range of 50–100 km, but its largest value is within the range of 50 km, although *RB* has fluctuations for the eight typhoon events when the range is larger than 300 km. Therefore, IMERG and TMPA mainly have the best applicability within the range of 50–100 km away from the typhoon tracks, and the worst applicability beyond a range of 300 km. This is also illustrated in Figures 4 and 5.

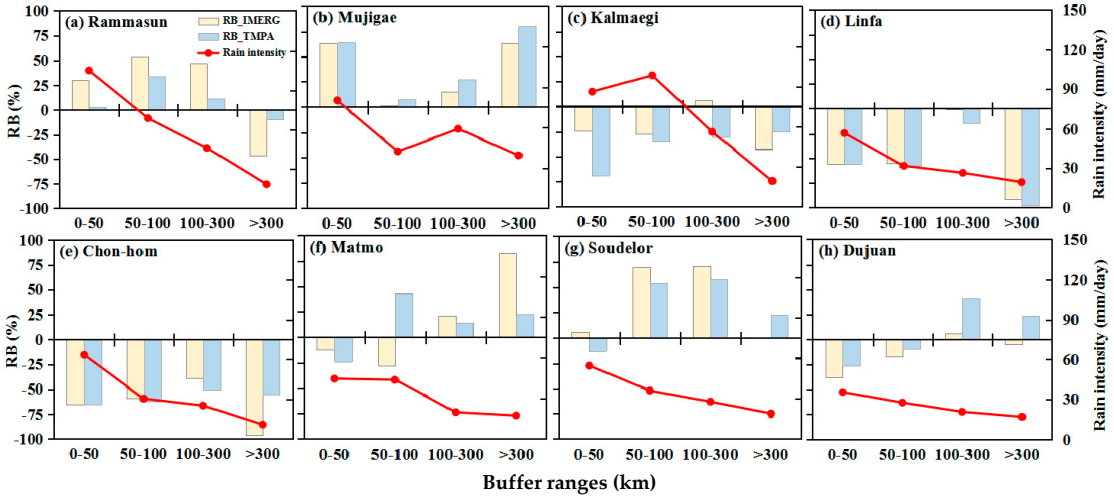

Figure 7. Variations of mean *RB* (%) and mean rain intensity (mm/day) within different buffer ranges (km) away from typhoon tracks during the period of (**a**) Rammasun, (**b**) Mujigae, (**c**) Kalmaegi, (**d**) Linfa, (**e**) Chon-hom, (**f**) Matmo, (**g**) Soudelor, and (**h**) Dujuan. The yellow histograms represent IMERG's mean *RBs*, and the blue histograms represent TMPA's mean *RBs*. The red polylines are the changes of mean rain intensity.

Table 4. Mean *RB* (%) of IMERG and TMPA within the different buffer ranges away from typhoon tracks.

Buffer Ranges (km)	IMERG								
	Group I				Group II				Mean
	Rammasun	Mujigae	Kalmaegi	Linfa	Chon-hom	Matmo	Soudelor	Dujuan	
<50	30.18	63.66	−24.11	−55.77	−65.57	−11.76	6.32	−37.47	−11.82
50–100	54.36	1.31	−17.26	−55.49	−58.78	−28.33	69.95	−17.47	−6.46
100–300	47.02	15.00	6.19	−1.13	−38.93	21.10	70.48	6.37	15.76
>300	−46.94	63.79	−42.82	−91.89	−96.40	82.81	0.84	−4.92	−16.94
Buffer Ranges (km)	**TMPA**								
	Group I				Group II				Mean
	Rammasun	Mujigae	Kalmaegi	Linfa	Chon-hom	Matmo	Soudelor	Dujuan	
<50	2.65	63.83	−69.00	−55.57	−65.57	−23.96	−13.21	−26.76	−23.45
50–100	34.03	7.64	−35.35	−57.20	−62.21	43.31	54.52	−9.42	−3.09
100–300	11.50	27.12	−30.00	−13.73	−50.51	14.50	58.09	40.88	7.23
>300	−9.30	79.40	−24.80	−98.11	−55.34	22.23	22.23	23.90	−4.97

5. Discussion

Why do both IMERG and TMPA generally perform better along the typhoon track than farther away from it? One possible explanation is its association with the physical structure of the typhoon and the underlying surface topography of typhoon tracks, both of which can influence the spatial distribution of rainfall intensity [42]. As shown in Figure 7, the mean rain intensity decreases with the increase of buffer ranges. Most storm centers are within the range of 50 km, where both IMERG and TMPA tend to underestimate the heavy rainfall. Meanwhile, when the range is larger than 300 km away from the typhoon track, there is light rain, for which the satellite products show large *RB* and have large uncertainties. Moreover, the impact range of typhoon-related heavy rain is also associated with the magnitude of each typhoon. This applicability range suggested in this study is just a simplified analysis and indicator of the error characteristics of satellite products in estimating typhoon heavy rain.

It has been reported that the current satellite rainfall products have limitations for monitoring typhoon heavy rain [43]. In particular, Chen et al. [44] found that TMPA 3B42V7 is least capable in the coastal region and significantly underestimates the heavy rainfall, which is the primary motivation of this study to investigate the performance of the latest released IMERG in the typhoon-affected coastal region and to compare its performance with TMPA 3B42V7. Our results also confirm this error pattern of both IMERG and TMPA in the coastal region of China. In addition, the daily rain gauge observations are used to validate the total rainfall estimated by both IMERG and TMPA. This is constrained by the availability of the hourly precipitation data in a large region in a timely way. Moreover, the density of the observation gauges in the studied area have impacts on the satellite-based rainfall errors. Thus, higher spatiotemporal density of gauges or gauge-satellite merged products could, potentially, be better in evaluating the errors and to monitor the evolution of heavy rainfall [32,45].

IMERG Level-3 and TMPA 3B42V7 are the emerging satellite precipitation products with relatively high resolutions in time and space, and have the potential to provide more reliable information for flood/drought monitoring, hydrologic modeling, and global climate change study. Previous studies [17,24,25] have demonstrated that the latest products have better performance, but few studies focused on typhoon-related heavy rain events that occur in a short time. That is another objective of this study to evaluate the performance of both products for typhoon rainfall. Overall, IMERG shows a better performance than TMPA.

6. Summary

This study compared the performance of the IMERG final run and TMPA 3B42V7 for typhoon heavy rain using ground gauge observations for reference, with focus on eight typhoon events that made landfall in the coastal region of China from July 2014 to October 2015. The main conclusive remarks are as follows:

1. All correlation coefficients (*CCs*) both of IMERG and TMPA for the investigated typhoon events are significant at the 0.01 level, but they tend to underestimate a total amount of heavy rainfall, especially around the storm center.
2. The IMERG final run shows an overall better performance than TMPA 3B42V7.
3. Both IMERG and TMPA exhibit a better performance (i.e., smaller absolute *RB*) when rain intensities are within 20–40 and 80–100 mm/day than those of 40–80 mm/day and larger than 100 mm/day. Meanwhile, both products generally have the best applicability in the range of 50–100 km away from typhoon tracks, and have the worst applicability beyond a 300-km range.
4. It needs to be emphasized that the study lacks physical insights to strengthen the statistical analysis. Future works, which will be devoted to further understand the limits of the applicability and accuracy of such satellite products in monitoring typhoon rainfall, should be focused on the physical process of typhoon rainfall, with consideration for the moving speed and direction of the typhoon, and the underlying topography.

Acknowledgments: This research was supported by the China National Key Technology R&D Program of 2015 (2015BAK11B02), the National Natural Science Foundation of China (41371055, 41611140112, and 41371404), and the Water Resource Science and Technology Innovation Program of Guangdong Province (#2016–19). We would like to express our appreciation to the Water Editorial Office, and two anonymous reviewers for their valuable comments and constructive suggestions.

Author Contributions: Ren Wang performed the experiments, processed the data, analyzed the results, and wrote the manuscript; Jianyao Chen conceived the experiments and contributed to the design of the manuscript; and Xingwei Wang improved the design of the experiments and the analysis of the results, and contributed to the writing of the manuscript.

Conflicts of Interest: The authors declare no conflict of interest.

References

1. Easterling, D.R.; Meehl, G.A.; Parmesan, C.; Changnon, S.A.; Karl, T.R.; Mearns, L.Q. Climate extremes: Observations, modeling, and impacts. *Science* **2000**, *289*, 2068–2074. [CrossRef] [PubMed]
2. Ban, N.; Schmidli, J.; Schar, C. Heavy precipitation in a changing climate: Does short-term summer precipitation increase faster? *Geophys. Res. Lett.* **2015**, *42*, 1165–1172. [CrossRef]
3. Yang, T.H.; Yang, S.C.; Ho, J.Y.; Lin, G.F.; Hwang, G.D.; Lee, C.S. Flash flood warnings using the ensemble precipitation forecasting technique: A case study on forecasting floods in Taiwan caused by typhoons. *J. Hydrol.* **2015**, *520*, 367–378. [CrossRef]
4. Habib, E.; Henschke, A.; Adler, R.F. Evaluation of TMPA satellite-based research and real-time rainfall estimates during six tropical-related heavy rainfall events over Louisiana, USA. *Atmos. Res.* **2009**, *94*, 373–388. [CrossRef]
5. Wang, X.; Xie, H.; Mazari, N.; Zeitler, J.; Sharif, H.; Hammond, W. Evaluation of a near-real time NEXRAD DSP product in evolution of heavy rain events on the Upper Guadalupe River Basin, Texas. *J. Hydroinform.* **2013**, *15*, 464–485. [CrossRef]
6. Prakash, S.; Mitra, A.K.; AghaKouchak, A.; Pai, D.S. Error characterization of TRMM Multisatellite Precipitation Analysis (TMPA-3B42) products over India for different seasons. *J. Hydrol.* **2015**, *529*, 1302–1312. [CrossRef]
7. Mehran, A.; AghaKouchak, A. Capabilities of satellite precipitation datasets to estimate heavy precipitation rates at different temporal accumulations. *Hydrol. Process.* **2014**, *28*, 2262–2270. [CrossRef]
8. Bharti, V.; Singh, C. Evaluation of error in TRMM 3B42V7 precipitation estimates over the Himalayan region. *J. Geophys. Res.* **2015**, *120*, 12458–12473. [CrossRef]
9. Collischonn, B.; Collischonn, W.; Tucci, C.E.M. Daily hydrological modeling in the Amazon basin using TRMM rainfall estimates. *J. Hydrol.* **2008**, *360*, 207–216. [CrossRef]
10. Hyun, J.Y.; Rockaway, T.D.; French, M.N. Ground-level rainfall variation in Jefferson County, Kentucky. *J. Hydrol. Eng.* **2016**, *21*, 05016029. [CrossRef]
11. Kitzmiller, D.; Miller, D.; Fulton, R.; Feng, D. Radar and multisensor precipitation estimation techniques in National Weather Service hydrologic operations. *J. Hydrol. Eng.* **2013**, *18*, 133–142. [CrossRef]
12. Huffman, G.J.; Adler, R.F.; Bolvin, D.T.; Gu, G.; Nelkin, E.J.; Bowman, K.P.; Hong, Y.; Stocker, E.F.; Wolff, D.B. The TRMM multisatellite precipitation analysis (TMPA): Quasi-global, multiyear, combined–sensor precipitation estimates at fine scales. *J. Hydrometeorol.* **2007**, *8*, 38–55. [CrossRef]
13. Kidd, C.; Huffman, G. Global precipitation measurement. *Meteor. Appl.* **2011**, *18*, 334–353. [CrossRef]
14. Hou, A.Y.; Skofronick-Jackson, G.; Kummerow, C.D.; Shepherd, J.M. Global precipitation measurement. In *Precipitation: Advances in Measurement, Estimation and Prediction*; Silas, M., Ed.; Springer: Belin/Heidelberg, Germany, 2008; pp. 131–169.
15. AghaKouchak, A.; Mehran, A.; Norouzi, H.; Behrangi, A. Systematic and random error components in satellite precipitation data sets. *Geophys. Res. Lett.* **2012**, *39*, L09406. [CrossRef]
16. AghaKouchak, A.; Nasrollahi, N.; Habib, E. Accounting for uncertainties of the TRMM satellite estimates. *Remote Sens.* **2009**, *1*, 606–619. [CrossRef]
17. Chen, S.; Hong, Y.; Gourley, J.J.; Huffman, G.J.; Tian, Y.; Cao, Q.; Yong, B.; Kirstetter, P.E.; Hu, J.; Hardy, J.; et al. Evaluation of the successive V6 and V7 TRMM multisatellite precipitation analysis over the Continental United States. *Water Resour. Res.* **2013**, *49*, 8174–8186. [CrossRef]
18. Goldstein, A.; Foti, R.; Montalto, F. Effect of spatial resolution in modeling stormwater runoff for an urban block. *J. Hydrol. Eng.* **2016**, *21*, 06016009. [CrossRef]
19. Liao, S.L.; Li, G.; Sun, Q.Y.; Li, Z.F. Real-time correction of antecedent precipitation for the Xinanjiang model using the genetic algorithm. *J. Hydroinform.* **2016**, *18*, 803–815. [CrossRef]
20. Huffman, G.J.; Bolvin, D.T.; Braithwaite, D.; Hsu, K.; Joyce, R.; Kidd, C.; Nelkin, E.J.; Xie, P. *Algorithm Theoretical Basis Document (ATBD) Version 4.4 for the NASA Global Precipitation Measurement (GPM) Integrated Multi-Satellite Retrievals for GPM (IMERG)*; NASA: Greenbelt, MD, USA, 2014; pp. 1–30.
21. Huffman, G.J.; Bolvin, D.T. TRMM and Other Data Precipitation Data Set Documentation. Available online: ftp://precip.gsfc.nasa.gov/pub/trmmdocs/3B42_3B43_doc.pdf (accessed on 13 April 2017).

22. Mitra, A.K.; Momin, I.M.; Rajagopal, E.N.; Basu, S.; Rajeevan, M.N.; Krishnamurti, T.N. Gridded daily Indian monsoon rainfall for 14 seasons: Merged TRMM and IMD gauge analyzed values. *J. Earth Syst. Sci.* **2013**, *122*, 1173–1182. [CrossRef]
23. Chen, S.; Hong, Y.; Cao, Q.; Gourley, J.J.; Kirstetter, P.E.; Yong, B.; Tian, Y.; Zhang, Z.; Shen, Y.; Hu, J.; et al. Similarity and difference of the two successive V6 and V7 TRMM multisatellite precipitation analysis performance over China. *J. Geophys. Res.* **2013**, *118*, 13060–13074. [CrossRef]
24. Tang, G.; Ma, Y.; Long, D.; Zhong, L.; Hong, Y. Evaluation of GPM Day-1 IMERG and TMPA Version-7 legacy products over Mainland China at multiple spatiotemporal scales. *J. Hydrol.* **2016**, *533*, 152–167. [CrossRef]
25. Tang, G.; Zeng, Z.; Long, D.; Guo, X. Statistical and hydrological comparisons between TRMM and GPM Level-3 products over a midlatitude basin: Is Day-1 IMERG a good successor for TMPA 3B42V7? *J. Hydrometeorol.* **2016**, *17*, 121–137. [CrossRef]
26. Sharifi, E.; Steinacker, R.; Saghafian, B. Assessment of GPM-IMERG and other precipitation products against gauge data under different topographic and climatic conditions in Iran: Preliminary results. *Remote Sens.* **2016**, *8*, 135. [CrossRef]
27. Guo, H.; Chen, S.; Bao, A.; Behrangi, A.; Hong, Y.; Ndayisaba, F.; Hu, J.; Stepanian, P.M. Early assessment of integrated multi-satellite retrievals for global precipitation measurement over China. *Atmos. Res.* **2016**, *176–177*, 121–133. [CrossRef]
28. Prakash, S.; Mitra, A.K.; Pai, D.S.; AghaKouchak, A. From TRMM to GPM: How well can heavy rainfall be detected from space? *Adv. Water Resour.* **2016**, *88*, 1–7. [CrossRef]
29. Chen, F.; Li, X. Evaluation of IMERG and TRMM 3B43 monthly precipitation products over Mainland China. *Remote Sens.* **2016**, *8*, 472. [CrossRef]
30. Liu, Z. Comparison of Integrated Multisatellite Retrievals for GPM (IMERG) and TRMM Multisatellite Precipitation Analysis (TMPA) monthly precipitation products: Initial results. *J. Hydrometeorol.* **2016**, *17*, 777–790. [CrossRef]
31. Sahlu, D.; Nikolopoulos, E.; Moges, S.; Anagnostou, E.; Hailu, D. First evaluation of the Day-1 IMERG over the upper Blue Nile Basin. *J. Hydrometeorol.* **2016**, *17*, 2875–2882. [CrossRef]
32. Wang, D.; Wang, X.; Liu, L.; Wang, D.; Huang, H.; Pan, C. Evaluation of CMPA precipitation estimate in the evolution of typhoon-related storm rainfall in Guangdong, China. *J. Hydroinform.* **2016**, *18*, 1055–1068. [CrossRef]
33. Kang, B. Statistical analysis of typhoon events in China. *China Flood Drought Manag.* **2016**, *26*, 36–40. (In Chinese).
34. China Typhoon Online. Available online: http://typhoon.weather.com.cn/ (accessed on 13 April 2017).
35. National Meteorological Center: Typhoon and Marine Weather Monitoring and Warning. Available online: http://typhoon.nmc.cn/web.html (accessed on 13 April 2017).
36. Toreti, A.; Kuglitsch, F.; Xoplaki, E.; Della-Marta, P.; Aguilar, E.; Prohom, M.; Luterbacher, J. A note on the use of the standard normal homogeneity test to detect inhomogeneities in climatic time series. *Int. J. Climatol.* **2011**, *31*, 630–632. [CrossRef]
37. Hirpa, F.A.; Gebremichael, M.; Hopson, T. Evaluation of high-resolution satellite precipitation products over very complex terrain in Ethiopia. *J. Appl. Meteorol. Clim.* **2010**, *49*, 1044–1051. [CrossRef]
38. NASA's Precipitation Measurement Missions. Available online: http://pmm.nasa.gov/data-access (accessed on 13 April 2017).
39. Skofronick-Jackson, G.; Huffman, G.; Stocker, E.; Walter, P. Successes with the Global Precipitation Measurement (GPM) Mission. In Proceedings of the Geoscience and Remote Sensing Symposium (IGARSS), Beijing, China, 10–15 July 2016; pp. 3910–3912.
40. Nastos, P.T.; Kapsomenakis, J.; Philandras, K.M. Evaluation of the TRMM 3B43 gridded precipitation estimates over Greece. *Atmos. Res.* **2016**, *169*, 497–514. [CrossRef]
41. Oliver, M.A.; Webster, R. Kriging: A method of interpolation for geographical information systems. *Inter. J. Geogr. Inf. Syst.* **1990**, *4*, 313–332. [CrossRef]
42. Huang, J.C.; Yu, C.K.; Lee, J.Y.; Cheng, L.W.; Lee, T.Y.; Kao, S.J. Linking typhoon tracks and spatial rainfall patterns for improving flood lead time predictions over a mesoscale mountainous watershed. *Water Resour. Res.* **2012**, *48*, W09540. [CrossRef]
43. Chen, Y.; Ebert, E.E.; Walsh, K.J.E.; Davidson, N.E. Evaluation of TRMM 3B42 precipitation estimates of tropical cyclone rainfall using PACRAIN data. *J. Geophys. Res.* **2013**, *118*, 2184–2196. [CrossRef]

44. Chen, S.; Hong, Y.; Cao, Q.; Kirstetter, P.E.; Gourley, J.J.; Qi, Y.; Zhang, J.; Howard, K.; Hu, J.; Wang, J. Performance evaluation of radar and satellite rainfalls for Typhoon Morakot over Taiwan: Are remote-sensing products ready for gauge denial scenario of extreme events? *J. Hydrol.* **2013**, *506*, 4–13. [CrossRef]
45. Shen, Y.; Zhao, P.; Pan, Y.; Yu, J. A high spatiotemporal gauge-satellite merged precipitation analysis over China. *J. Geophys. Res.* **2014**, *119*, 3063–3075. [CrossRef]